

# Shear zones and wall slip in the capillary flow of concentrated colloidal suspensions

Lucio Isa, Rut Besseling, and Wilson C K Poon

*SUPA & School of Physics, The University of Edinburgh, James Clerk Maxwell Building,  
The Kings Buildings, Mayfield Road, Edinburgh EH9 3JZ, UK*

(Dated: March 23, 2022)

We image the flow of a nearly random close packed, hard-sphere colloidal suspension (a ‘paste’) in a square capillary using confocal microscopy. The flow consists of a ‘plug’ in the center while shear occurs localized adjacent to the channel walls, reminiscent of yield-stress fluid behavior. However, the observed scaling of the velocity profiles with the flow rate strongly contrasts yield-stress fluid predictions. Instead, the velocity profiles can be captured by a theory of stress fluctuations originally developed for chute flow of dry granular media. We verified this behavior both for smooth and rough boundary conditions.

PACS numbers: 83.80.Hj, 83.50.Ha, 83.60.La

Understanding the deformation and flow, or rheology, of complex fluids in terms of their constituents (colloidal particles, polymer chains or surfactant aggregates) poses deep challenges to fundamental physics, and has wide industrial applications [1]. The experimental study of complex fluid rheology typically starts in a rheometer, in which stresses and strains are applied and measured in well-defined, ‘rheometric’ geometries (‘cone-plate’, etc.). Translating rheometer data to more complex flows is non-trivial, but well developed in polymers (see, e.g., [2]).

The understanding of colloidal flows lags considerably behind and despite their equal practical importance [3, 4], studies on model systems have been carried out only recently [5]. Compared to polymers, colloids pose some unique challenges. Concentrated suspensions (‘pastes’) are generally non-ergodic (or ‘glassy’), so that *any* flow involves non-linearities (e.g. yielding [6, 7] or shear thickening [8, 9]). Moreover, specific geometries in applications may involve dimensions comparable to single particles and lead to confinement effects, such as in micro-fluidics [10]. The most quantitative theory for quiescent colloidal glasses, mode coupling theory, has only recently been extended to deal with simple shear [11].

Here we present an experimental study of the flow of a hard-sphere suspension at nearly random close packing, a ‘paste’, in a twenty-particle-wide square capillary. Pastes are ubiquitous in industry, where their unique rheology presents many challenges and opportunities [4]. The simplicity of the geometry is appealing from the fundamental perspective. It also makes direct contact with microfluidic applications [10]. Using fast confocal microscopy, we tracked the motion of individual colloids and measured the velocity profiles in channels with both smooth and rough walls. Despite the colloidal nature of our suspension, we find significant similarities with granular flow, itself of wide applied [12] and fundamental [13] interest.

We used sterically stabilised polymethylmethacrylate (PMMA) spheres of diameter  $D = 2.6 \pm 0.1 \mu\text{m}$  (from confocal microscopy) fluorescently labelled with nitrobenzoxadiazole, and suspended in a mixture of cycloheptylbromide and mixed decalin (viscosity 2.6 mPa·s) for buoyancy matching at room temperature  $T = T_r$ .

Their Brownian time is  $\tau_B = D^2/24D_0 \simeq 4.4 \text{ s}$  with  $D_0$  the bare diffusion coefficient.

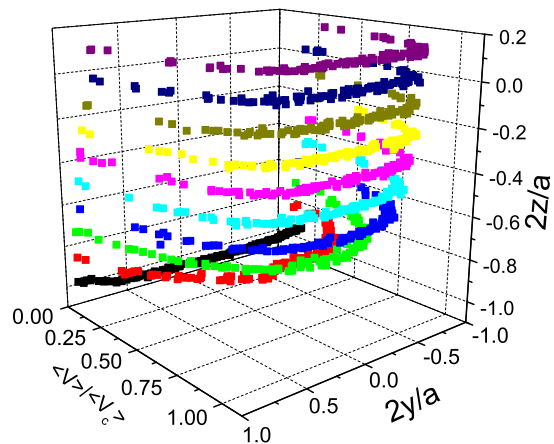


FIG. 1: Velocity profiles in the lower half of the capillary (width  $2a = 50 \mu\text{m}$ ) with smooth walls reconstructed in  $3 \mu\text{m}$  steps. The average velocity  $\langle V \rangle$  is in units of the average velocity of the central, unsheared, ‘plug’,  $\langle V_c \rangle = 20 \mu\text{ms}^{-1}$ .

A dense suspension (volume fraction  $\phi \gtrsim 0.63$ , from confocal microscopy) was obtained by centrifuging (at  $T > T_r$  to remove buoyancy matching). A constant pressure gradient,  $\nabla p$ , is applied to drive the suspension into a square borosilicate glass micro-channel (Vitrocom Ltd; side  $2a = 50 \mu\text{m}$ ) [14], whose inner walls were either untreated and smooth, or coated with a disordered monolayer of colloids and thus rough on the particle level. The coating particles, which are slightly larger ( $\bar{D}_{\text{coat}} = 2.8 \mu\text{m}$ ) and more polydisperse PMMA spheres (right inset to Fig. 3), were applied by filling with a dilute suspension and attached by heating in a vacuum oven ( $110^\circ\text{C}$ ).

The flow (along  $x$ ) across the full width of the channel ( $|y| \leq a$ ) was imaged with a Visitech VTeye confocal scanner in a Nikon TE Eclipse 300 inverted microscope. We collected  $44 \mu\text{m} \times 58 \mu\text{m}$  images (107 frames per second) at depths  $-a < z < +0.2a$  ( $z = -a$  is the lower surface). From the two-dimensional images, we located par-

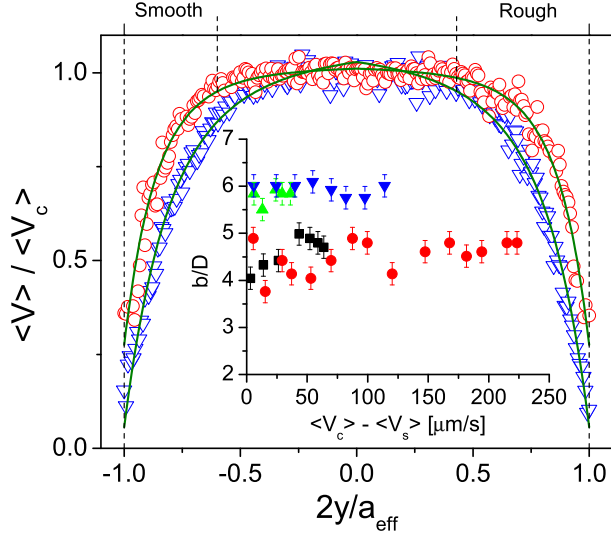


FIG. 2: Averaged velocity profile as a function of  $2y/a_{\text{eff}}$  for smooth ( $\circ$ ) and rough ( $\nabla$ ) walls at  $z = 17 \mu\text{m}$ . Full lines: fits from integrating Eq. 7; dotted lines: extents of sheared zones.  $\langle V_c \rangle$  is  $114 \mu\text{ms}^{-1}$  for the smooth wall case and  $80 \mu\text{ms}^{-1}$  for the rough wall case. Inset: width of shear zone in units of particle diameter as a function of  $\Delta V$ .  $\blacktriangle$  and  $\blacktriangledown$ : two runs for rough walls;  $\bullet$  and  $\blacksquare$ : two runs for smooth walls.

ticles with a resolution  $\delta x, \delta y \simeq 50 \text{ nm}$  [15]. A key step for correct tracking is to follow colloids in a ‘comoving’ frame [14]. This involves removing from the ‘raw’ coordinates the advective motion  $\Delta x(\bar{y})$ , which is obtained as the  $x$ -shift that maximizes the cross correlation between image strips around  $\bar{y}$  in successive frames. From time-dependent coordinates (restored in the lab frame), we obtained particle velocities [25]. After start-up transients, we found oscillations in the particle velocities (data not shown) at 0.1 Hz (slow flow) to 1 Hz (fast flow). This feature, which we discuss elsewhere, is ubiquitous in the pipe flow of pastes [5, 16]. Here, we restrict ourselves to steady-state velocity profiles,  $\langle V \rangle$ , obtained by averaging over 20 s (slow flow) to 10 s (fast flow), corresponding to  $\sim 2000$  to  $\sim 1000$  frames, respectively. We imaged at  $x \sim 0.5 \text{ cm}$  from the entrance to the capillary (corresponding to  $\sim 2000$  particles), where entry effects have died out and the results show negligible  $x$  dependence.

Typical data for smooth walls are shown in Fig. 1. For  $z \gtrsim 10 \mu\text{m}$ , each velocity profile consists of a shear zone close to the walls and a nearly unsheared central ‘plug’. This plug shrinks at smaller  $z$ , i.e. closer to the bottom wall. We also observe wall slip with velocity  $\langle V_s \rangle$ . The profiles for smooth and rough walls, Fig. 2, are qualitatively similar, but the latter displays considerably smaller wall slip and larger shear zones. Note that for rough walls, we use an effective half width  $a_{\text{eff}} = a - \bar{D}_{\text{coat}} - \bar{D}/2$ ; for smooth walls,  $a_{\text{eff}} = a - \bar{D}/2$ .

The dependence of the velocity profiles on the overall flow rate is striking. We define the width of the shear zone  $b$  as the distance from the wall where the flow speed

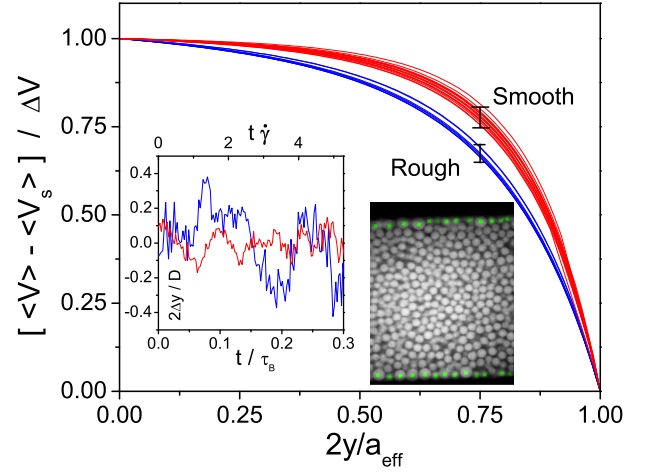


FIG. 3: Normalized velocity profiles at  $z = 17 \mu\text{m}$  versus  $2y/a_{\text{eff}}$ . We use the profiles fitted from integrating Eq. 7; the error bars show the spread in the measured data. Left inset: normalized transverse fluctuations of individual particles in the shear zone for the two boundary conditions, versus normalized time  $t/\tau_B$  or local accumulated strain  $t \cdot \partial \langle V(y) \rangle / \partial y = t \cdot \dot{\gamma}(y)$ , top axis. The traces show larger fluctuations in the rough wall case. Right inset: confocal microscopy snapshot of the flow at  $z = 17 \mu\text{m}$  for a channel with rough walls; the particles marked with  $\bullet$  are attached to the walls.

is  $\langle V_s \rangle + 0.95 \Delta V$  where  $\Delta V = \langle V_c \rangle - \langle V_s \rangle$  is the difference between the averaged center and wall speeds (with  $\Delta V/a$  the average shear rate). We see in the inset to Fig. 2 that  $b$  is independent of  $\Delta V$ , i.e. the central plug remains essentially constant for flow rates varying by more than one decade. Associated with this, the normalized velocity profiles  $(\langle V \rangle - \langle V_s \rangle) / \Delta V$  for different flow rates collapse onto two different master curves for rough and smooth walls, Fig. 3.

Let us now compare the observed behavior to what is expected from bulk rheology. Considering the system as a glassy yield stress fluid, the stress  $\tau$  versus strain rate  $\dot{\gamma}$  relation typically displays Herschel-Bulkley shear thinning behavior:  $\tau - \tau_{\text{yield}} \propto \dot{\gamma}^n$  ( $n \approx 0.5$ ) [6] with  $\tau_{\text{yield}}$  the yield stress. Plug flow is ubiquitous in all yield stress fluids, and has been extensively studied [17]. Thus, our observation of plug flow is, in itself, unsurprising. In yield stress fluids though, if the maximum applied shear stress in the channel exceeds  $\tau_{\text{yield}}$ , we have plug flow with shear zones whose boundaries are given by  $\tau = \tau_{\text{yield}}$ ; hence, the width of the shear zone,  $b$ , grows with the shear rate and eventually leaves a vanishingly small ‘plug’ [17]. *This is not what we observe.*

A clue to what may be happening in our experiments comes from the observation that at the typical strain rate encountered in the shear zones,  $\tau_B(\Delta V/a) \sim 50$ , conventional rheology would lead us to expect severe shear thickening. Shear thickening in pastes is very far from completely understood on the microscopic level [8, 18, 19]; but we may speculate that for colloids stabilised by short grafted polymers, interparticle friction

may become important as they jam against each other driven by shear. Indeed, the measured transverse fluctuations of particles clearly show the motions induced by them ‘bumping’ along neighboring layers, Fig. 3 inset. We are thus led to consider analogies with friction-dominated granular flow.

Indeed, both the width of the shear zone  $b \sim 6D$  ( $\sim 5D$  for smooth walls) and the lack of flow rate dependence, are strongly reminiscent of observations in gravity-driven ‘chute flow’ of dry granular materials [20]. In particular, Pouliquen and Gutfraind observed  $b \approx 6D$  in the two-dimensional flow of discs (diameter  $D$ ) for channels of widths  $10D \leq 2a \leq 44D$  and developed a model to account for their observations [20, 21]. Below we extend their model to three dimensions, and show that it indeed predicts  $b$  independent of  $\Delta V$ .

Following [20] we start with the components of the stress tensor  $\boldsymbol{\tau}$  in the fully-developed flow of a continuum medium in the  $x$  direction along a pipe, which satisfies

$$\frac{\partial \tau_{xx}}{\partial x} + \frac{\partial \tau_{xy}}{\partial y} + \frac{\partial \tau_{xz}}{\partial z} = 0, \quad (1)$$

$$\frac{\partial \tau_{yy}}{\partial y} = \frac{\partial \tau_{zz}}{\partial z} = 0, \quad (2)$$

with  $\partial \tau_{xx} / \partial x = -\nabla p$ . For a square pipe of side  $2a$  [22]:

$$\begin{aligned} \tau_{xy}(z) = \tau_0 \sum_{k=1,3,5,\dots}^{\infty} (-1)^{(k+1)/2} \times \\ \times \left[ 1 - \frac{\cosh(k\pi z/2a)}{\cosh(k\pi/2)} \right] \frac{\sin(k\pi y/2a)}{k^2} \end{aligned} \quad (3)$$

where  $\tau_0 = 8a\nabla p / \pi^2$ . This constant sets the scale for the ( $z$ -dependent) maximum stress at the wall,  $\tau_{\max}$ .

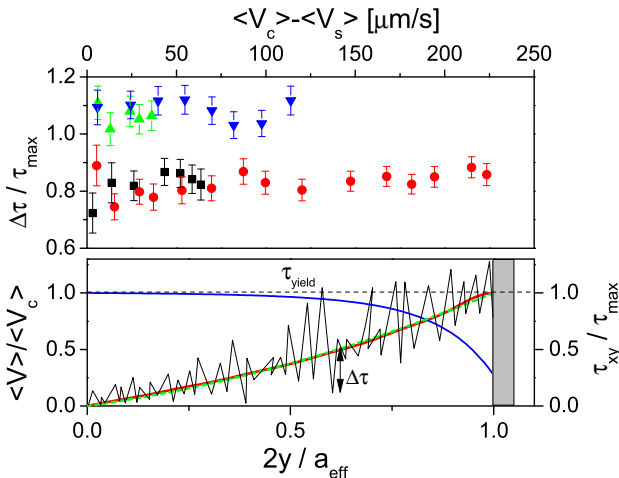


FIG. 4: (Top) Fitted fluctuating stress amplitude  $\Delta\tau$  in units of  $\tau_{\max}$  as a function of the ‘net shear’,  $\Delta V$ ; symbols as in Fig. 2. (Bottom) Schematic of the fluctuating shear stress superimposed on the continuum  $\tau_{xy}$ . The dashed line shows the quadratic fit used for the integration. In the zone where the fluctuating stress overcomes  $\tau_{\text{yield}}$ , flow results.

To determine the normal stress,  $\tau_{yy}$  we impose a Coulomb friction condition at the walls:

$$\tau_{yy} = \mu_{\text{wall}}^{-1} \tau_{\max}, \quad (4)$$

where  $\mu_{\text{wall}}$  is the friction coefficient between the suspended particles and the wall; this constant  $\tau_{yy}$  satisfies Eq. 2 [26]. Following the Coulomb criterion, the material yields if  $\tau_{xy} \geq \tau_{\text{yield}} \equiv \mu_{\text{bulk}} \tau_{yy}$ , with  $\mu_{\text{bulk}}$  the friction coefficient inside the material. We expect  $\mu_{\text{wall}} \leq \mu_{\text{bulk}}$ , with ‘=’ for a rough wall coated with particles, and ‘<’ for smooth, glass walls. From Eq. 4 we have:

$$\tau_{\text{yield}} = (\mu_{\text{bulk}} / \mu_{\text{wall}}) \tau_{\max} \geq \tau_{\max}. \quad (5)$$

Since  $\tau_{xy} \leq \tau_{\text{yield}}$ , the bulk never yields and the whole material slips as a plug. Note from Eq. 5 that  $\tau_{\text{yield}}$  increases with  $\tau_{\max}$  (and therefore  $\Delta V$ ). This reflects the rising normal stress  $\tau_{yy}$ , Eq. 4, which increases the friction between particles and thus  $\tau_{\text{yield}}$  [27].

We now assume the presence of stress fluctuations which, when added to the continuum  $\tau_{xy}$ , Eq. 3, may take the local stress above  $\tau_{\text{yield}}$ , Fig. 4. Following [20] we use a ‘Boltzmann’ ansatz for the yielding probability:

$$p_{\text{yield}} \propto \exp \left[ -\frac{|\tau_{\text{yield}}(z) - |\tau_{xy}(y, z)||}{\Delta\tau} \right], \quad (6)$$

where  $\Delta\tau \equiv \Delta\tau(z)$  is the amplitude of stress fluctuations, taken to be independent of  $y$  at any particular  $z$ . The model is completed by the simplest possible ansatz relating shear rate to  $p_{\text{yield}}$ :  $\partial V(y, z) / \partial y \propto p_{\text{yield}}$  [28]. At a fixed  $z = z_0$ , therefore, we have

$$\frac{\partial V(y, z_0)}{\partial y} = \text{constant} \times \exp \left[ \frac{\tau_{xy}(y, z_0)}{\Delta\tau} \right]. \quad (7)$$

In order to perform the integration analytically we fitted the stress profile, Eq. 3, with a quadratic approximation; Fig. 4 (bottom) shows both the analytic expression and the fit. We then substituted the fitted stress into Eq. 7, integrated and fitted the resulting velocity profile to the measured data. Example results are shown in Fig. 2.

The fitted stress fluctuation amplitudes normalized to the wall stress,  $\Delta\tau / \tau_{\max}$ , at  $z = 17 \mu\text{m}$  for both smooth and rough walls are plotted against  $\Delta V$  in Fig. 4. As  $\tau_{\max}$  increases with flow rate,  $\Delta\tau$  increases proportionally so that their ratio remains constant. Combined with Eqs. 3 and 5 this means that  $(\tau_{\text{yield}} - |\tau_{xy}|) / \Delta\tau$  in Eq. 6 is independent of  $\tau_{\max}$ , resulting in a constant value for  $b$ , Fig. 2, and collapse of the velocity profiles, Fig. 3.

The fact that  $\Delta\tau$  scales as the wall stress  $\tau_{\max}$  suggests that the stress fluctuations are controlled by what happens at the boundaries. Two dimensional simulations of dry granular matter indeed relate stress fluctuations to inhomogeneities in the friction-dominated force chains resulting from contacts at the walls [23]. Here, we find (for  $z \sim a$ ) that  $\Delta\tau / \tau_{\max}$  for rough walls is somewhat larger than for smooth walls, Fig. 4; this difference is directly correlated with the observed difference in  $b$ , Fig. 2.

The presence of such a difference, and its sign, is unsurprising. Flow along a smooth wall is less ‘bumpy’ and can thus be expected to generate a lower level of stress fluctuations which propagate through the system, as also shown by the two traces in the left inset to Fig. 3 [29].

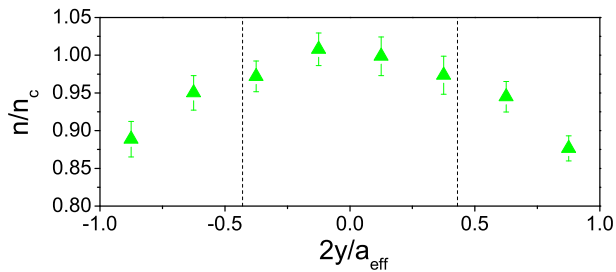


FIG. 5: Average density profile at  $z = 17 \mu\text{m}$  for rough walls, in units of the density  $n_c$  in the center. Dashed lines: average width  $b$  of the shear zones in channels with rough walls.

The analogy with granular flow extends further than the constant shear zone width. In [20], a variation of the density across the channel was observed, the ‘plug’ being  $\sim 10\%$  denser than the edge of the shear zone. We observe the same feature in our channel flows. Figure 5 shows a typical density profile at  $z = 17 \mu\text{m}$ , measured by counting particles per unit area and averaging  $10^4$  frames; this profile is essentially independent of the overall flow rate. The observed density reduction in the shear zone is not unexpected, since dilatancy is required in flowing

particulates (dry or wet) at such high packing fractions.

Our findings also have implications concerning the role played by confinement. Since  $D/2a \approx 20$ , one might expect strong size-dependence. However, the width of the shear zone  $b$  we observed, is always smaller than the width of the channel,  $a$  and size effects should only become significant for channels with  $a \lesssim b$ .

To summarize, we have measured the flow properties of a nearly-random-close-packed hard-sphere colloid driven by a constant pressure gradient in a twenty-particle-diameter square channel by tracking the motion of individual particles using fast confocal microscopy. At all flow rates, we observed a central, almost unsheared plug, and peripheral shear zones. In contrast to the prediction of yield-stress fluid rheology, the size of the shear zone remained constant as the flow rate was increased. We explained this by appealing to a model originally set up for the gravity-driven ‘chute flow’ of dry granular materials [20]. This model should be applicable in our case if the yield stress,  $\tau_{\text{yield}}$ , is dominated by inter-particle friction. The model predicts that stress fluctuations can bring about yielding even when the average stress is below  $\tau_{\text{yield}}$ . Quantitative fits to our data were obtained.

We thank Andrew Schofield for providing the particles, and Eric Weeks and Alexander Morozov for helpful discussions. L. Isa was funded by the EU network MRTN-CT-2003-504712, and R. Besseling by EPSRC GR/S10377/01 and EP/D067650/1.

- 
- [1] R. G. Larson, *The Structure and Rheology of Complex Fluids* (Oxford University Press, Oxford, 1999).
  - [2] J. Bent et al., *Science* **301**, 1691 (2003).
  - [3] J. A. Lewis, *J. Am. Ceramic Soc.* **83**, 2341 (2000).
  - [4] D. I. Wilson et al., *Chem. Engin. Sci.* **61**, 4147 (2006).
  - [5] M. D. Haw, *Phys. Rev. Lett.* **92**, 185506 (2004).
  - [6] G. Petekidis et al., *J. Phys.-Condens. Mat.* **16**, S3955 (2004).
  - [7] K. N. Pham et al., *Europhys. Lett.* **75**, 624 (2006).
  - [8] W. J. Frith et al., *J. Rheo.* **40**, 531 (1996).
  - [9] D. Lootens et al., *Phys. Rev. Lett.* **90**, 178301 (2003).
  - [10] D. Psaltis et al., *Nature* **442**, 381 (2006).
  - [11] M. Fuchs and M. E. Cates, *Phys. Rev. Lett.* **89**, 248304 (2002).
  - [12] C. S. Campbell, *Powder Technol.* **162**, 208 (2006).
  - [13] G. D. R. MiDi, *Eur. Phys. J. E* **14**, 341 (2004).
  - [14] L. Isa et al., *J. Phys.-Conference Series* **40**, 124 (2006).
  - [15] J. C. Crocker and D. G. Grier, *J. Colloid Interface Sci.* **179**, 298 (1996).
  - [16] P. Yaras et al., *Rheol. Acta* **33**, 48 (1994).
  - [17] R. R. Huilgol and Z. You, *J. Non-Newton. Fluid Mech.* **128**, 126 (2005).
  - [18] M. E. Cates et al., *Phys. Rev. Lett.* **81**, 1841 (1998).
  - [19] R. C. Ball and J. R. Melrose, *Adv. Colloid Interfac.* **59**, 19 (1995).
  - [20] O. Pouliquen and R. Gutfriend, *Phys. Rev. E* **53**, 552 (1996).
  - [21] O. Pouliquen, *Phys. Rev. Lett.* **93**, 248001 (2004).
  - [22] F. M. White, *Viscous Fluid Flow* (McGraw-Hill, 1991), 2nd ed.
  - [23] R. Gutfriend and O. Pouliquen, *Mech. Mater.* **24**, 273 (1996).
  - [24] M. Frank et al., *J. Fluid Mech.* **493**, 363 (2003).
  - [25] This procedure applied to the flow of a 30% suspension in a two-dimensional channel gave parabolic profiles [14] as also found in [24].
  - [26] A completely analogous discussion can be given for  $\tau_{xz}$  and  $\tau_{yz}$ , leading to a velocity profile  $V(z)$ .
  - [27] Thus, this *variable* Coulombic yield stress is a different quantity from the *constant* yield stress featuring in (say) the HB model.
  - [28] The ansatz 6 was proposed [20] to account for shear-zone behavior next to walls, and is qualitatively incorrect for the center of the pipe, where we must have  $\partial V/\partial y = 0$ .
  - [29] We also note that for smooth walls we find considerable layering in the structure close to the walls [14].